ФИЗИКА ЭЛЕМЕНТАРНЫХ ЧАСТИЦ И АТОМНОГО ЯДРА
2013. Т. 44. ВЫП. 3

BFKL EVOLUTION AS A COMMUNICATOR BETWEEN SMALL AND LARGE ENERGY SCALES

H. Kowalski [1], *L. N. Lipatov*[2], *D. A. Ross*[3]

[1] Deutsches Elektronen-Synchrotron DESY, Hamburg, Germany

[2] Petersburg Nuclear Physics Institute, Gatchina, St. Petersburg, Russia

[3] School of Physics and Astronomy, University of Southampton, Highfield, Southampton, UK

We analyze, in leading and next-to-leading order of the BFKL equation, the effects of the quantization of the singularities of the j-plane, t-channel partial waves due to the imposition of appropriate infrared and ultraviolet boundary conditions. We show that the intercepts ω_n of the Regge poles, which contribute significantly to the gluon density in the kinematic region measured at HERA and which can be calculated in QCD and in a supersymmetric extension of QCD, are substantially modified by the Beyond Standard Model (BSM) effects. We also develop a physically motivated heuristic model for the infrared boundary condition and apply it to the gluon density. We argue that, using this type of model, the analysis of present and future low-x data could allow one to detect supersymmetry at a high energy scale.

PACS: 12.38.Cy

1. INTRODUCTION

The BFKL equation determines the high-energy behaviour of the virtual gluon–gluon scattering amplitude in Regge limit, in which the cms energy $\sqrt{s}$ is much larger than the transverse momenta k, k' of the gluons. It was derived in the fixed coupling constant case by resumming *all* the Feynman diagrams describing gluon–gluon scattering in the leading or next-to-leading order. The scattering amplitude displays a scale invariance such that it can be described solely by functions of ratios of transverse momenta k and k'.

A common application [1–3] of the BFKL equation is to use it as an evolution equation in rapidity y and transverse momentum k for some large-rapidiity amplitude, namely,

$$\frac{\partial}{\partial y}\mathcal{A}(y,t) = \int dt' \mathcal{K}(\bar{\alpha_s}, t, t')\mathcal{A}(y,t'), \tag{1.1}$$

where

$$t = \ln\left(\frac{k^2}{\Lambda^2_{\rm QCD}}\right).$$

and the coupling $\bar{\alpha_s}$ runs with transverse momentum. This application is often used as it lends itself relatively easily to an extension of the DGLAP formalism to very low values of Bjorken-x, where the pure DGLAP formalism is known to break down.

In order to solve this evolution equation, one requires as input the amplitude at some rapidity y for all values of transverse momentum t'. One could naively expect that Eq. (1.1) could be directly solved for large y and t well in the perturbative region because it is known that the BFKL kernel $K(t,t')$ is quasi-local in t; i.e., it diminishes when $|t-t'|$ is large. However, as was carefully investigated, e.g., in [1], the BFKL equation is not only an evolution in y but also in virtualities t, which leads to a substantial diffusion into the low transverse momenta region where perturbative QCD cannot be valid. Therefore, the authors of [1] proposed a modification of the BFKL equation by imposing a low and high cutoff in t on the BFKL integral, a procedure which is today widely accepted. However, such a cutoff implies that the amplitude actually vanishes below a certain transverse momentum, rather than becoming nonperturbative. In fact, due to the growth of the coupling constant at small k_T, the amplitude could grow in this region and the vanishing of it at the infrared cutoff looks unnatural.

In [4] we proposed to solve Eq. (1.1) by the Green function method which does not require any cutoff on the BFKL integral. Instead, we assumed that the nonperturbative infrared region of QCD imposes a certain phase on the oscillatory parts of the eigenfunctions at some small transverse momentum. This treatment of the infrared boundary leads to a discrete set of eigenvalues, ω_n, of the BFKL kernel, since only certain values permit the construction of eigenfunctions which simultaneously obey these phase conditions at low transverse momentum *and* the large transverse momentum boundary conditions imposed by the asymptotic freedom. This is in contrast to the «usual» treatment [1–3], in which a lower transverse momentum cutoff is imposed on the amplitude; i.e., the amplitude is assumed to vanish below the cutoff. In our approach, the amplitudes are particularly sensitive to the exact values of the discrete ω_n which are related to the nonperturbative phases η_n at the cutoff. These phases are determined, in turn, by the gluon–gluon interactions of the nonpertubative QCD, which lead to rich structures below this cutoff.

A rigid cutoff (either UV or IR) destroys the scale invariance of the BFKL kernel and hence the validity of scale-covariant solutions. As pointed out in [1], the imposition of such cutoffs has no effect on the position of the leading singularity (the exponent of x in structure functions) but does affect the prefactor, which is controlled by the form of this singularity. We find that the subleading singularities are also essential in order to obtain a good fit to HERA data. In our application of BFKL dynamics, the scale and conformal invariance (which is central to the BFKL formalism for fixed coupling) is broken in a controlled way, namely, only through the running of the coupling and we assume «quasi-

conformal» solutions in which the exponent of the transverse momentum varies slowly in order to compensate for the change in the coupling in accordance with a generalized DGLAP dynamics.

In our previous paper [4] we have shown that HERA F_2 data, at low x, can be described very well by the gluon density constructed from the discrete spectrum of eigenfunctions of the BFKL kernel. The spectrum contained many eigenfunctions, $\mathcal{O}(100)$, with eigenvalues ω_n varying from $\omega_1 \sim 0.25$ to $\omega_n \sim 0.5/n$ for large n. This first successful confrontation of the BFKL formalism [6] with data led to the unexpected question as to whether the HERA data are sensitive to the Beyond Standard Model (BSM) effects. These effects, although only present at scales that are much higher than the region of HERA data, can nevertheless affect the quality of the fits to data since BSM effects change the running of the coupling and consequently also substantially change the values of ω_n.

This seems somewhat counter-intuitive. One may ask how it can be possible that a fit to data at relatively low energies can be sensitive to corrections due to loops of particles whose masses are far in excess of those energies. The crucial point is that the above-mentioned large transverse momentum boundary conditions, imposed by the running of the coupling, can occur at very high k_T scales*. For $\omega <\sim 0.1$ this is already above the scale at which one might expect BSM physics to occur. The value of the discrete eigenvalues arises from an interplay between these ultraviolet boundary conditions and the infrared boundary condition arising from the imposition of an infrared phase. It is in this sense that in our treatment of the BFKL formalism there is communication between high- and low-energy scales. We make the assumption that the allowed eigenvalues can be obtained from the BFKL equation supplemented by an infrared phase condition in a *process-independent* way, i.e., without needing to impose any infrared or ultraviolet cuts on the integration over transverse momentum. Once these eigenvalues are calculated, their corresponding eigenfunctions are convoluted with the necessary impact factors in order to obtain the required amplitudes. In this way, it turns out that even though these amplitudes, in accordance with kinematical constraints, never involve diffusion into transverse momenta above the threshold for BSM physics, the rapidity dependence of such amplitudes is affected by the substantial changes in the eigenvalues arising as a result of BSM physics.

To understand how the running of the coupling constant can have such far reaching consequences, we derive analytically (in Sec. 2) the main properties of the discrete pomeron solution using the LO BFKL equation. This derivation provides a qualitative physical explanation of the mechanism by which the BSM

*Note that this means that formally we determine the eigenvalues at asymptotically large initial energies.

effects modify the discrete pomeron structures and lead to a genuine change of the eigenvalues and eigenfunctions. It also elucidates the role of the infrared phases which define the boundary condition and which can be *indirectly determined* from data. This explanation is then carried over into the NLO evaluation, which was used for data analysis and was performed numerically.

As a popular example of BSM effects, we have chosen the $N = 1$ supersymmetry and modified the β function and the kernel of the BFKL equation to include the contributions from the superpartners. We then describe the full NLO evaluation of the Discrete BFKL Pomerons (DP) with collinear resummation [10]. This allows us to show that the eigenvalues ω_n, at larger n, have a genuine sensitivity to BSM physics because the support of the corresponding eigenfunctions extends to very high virtualities. The values of ω_n are determined (to large extent) by the running of α_s and the properties of the BFKL kernel in the high virtuality regions, where BSM effects dominate and QCD NLO corrections are very small. This is also the reason why these eigenvalues are not sensitive to a particular choice of the infrared boundary. All these properties are discussed in detail in Sec. 2.

In Sec. 3 we then show that it is possible to construct a physically self-consistent infrared boundary condition which determines the properties of the gluon density to be in agreement with data. Finally, we confront the DP gluon density with the HERA F_2 data and show that within our model for the infrared boundary condition we obtain indirect evidence of a supersymmetric threshold in a multi-TeV range.

In Sec. 4 we discuss our results with particular emphasis on the role of the universal Green function and the momentum conservation. We also discuss the dependence of our fits on the choice of the infrared boundary condition. Section 5 presents a summary.

2. THE DISCRETE BFKL POMERON

The forward amplitude for a diffractive process with rapidity (or rapidiy gap) y is determined by the QCD pomeron and may be written as

$$\mathcal{A}(y) = \int d\omega \int dt \int dt' \Phi_u(t)\, \Phi_d(t') x^{-\omega} \tilde{\mathcal{G}}_\omega(t, t'), \tag{2.1}$$

where $\tilde{\mathcal{G}}_\omega(t, t')$ is the Mellin transform of a universal (i.e., process-independent) Green function $\mathcal{G}(t, t', y - y')$,

$$\mathcal{G}(t, t', y - y') = \int d\omega\, \tilde{\mathcal{G}}_\omega(t, t')\, \mathrm{e}^{\omega(y-y')}. \tag{2.2}$$

The process dependence enters only through the impact factors Φ'_u, Φ_d at the top and bottom of the gluon ladder which depend on the transverse momenta of the

gluons and may also depend on other kinematic variables. The integral over ω in the inverse Mellin transform, (2.2), is performed over a contour parallel to the imaginary axis, to the right of all singularities of the Green function. This Green function obeys the equation

$$\omega\tilde{\mathcal{G}}_\omega(t,t') - \int dt''\,\mathcal{K}(\bar{\alpha_s},t,t'')\,\tilde{\mathcal{G}}_\omega(t'',t') = \delta(t-t'), \tag{2.3}$$

which is solved by determining the set of eigenfunctions of the BFKL kernel, subject to certain boundary conditions. If we allow the coupling $\bar{\alpha_s}$ to run with t,t', which in LO means replacing it by $\sqrt{\bar{\alpha_s}(t)\bar{\alpha_s}(t')}$, then, as we explain below, the UV boundary condition, namely that the eigenfunctions decay as $t\to\infty$, is automatically implemented. The infrared boundary condition is imposed by requiring that the eigenfunctions have some given nonperturbative phases at some low value of t^*. As was first shown in [12] and we explain again below, the combination of the UV boundary condition (which determines the oscillation phase at $t=t_c$, where the oscillatory behaviour changes to an exponentially decaying behaviour, compatible with a DGLAP analysis in the double logarithmic limit) and the infrared phase condition leads (for positive ω) to a discrete set of allowed eigenvalues ω_n with their attendant eigenfunctions, so that the Green function may be written as

$$\tilde{\mathcal{G}}_\omega(t,t') = \sum_n \frac{f^*_{\omega_n}(t')f_{\omega_n}(t)}{\omega-\omega_n} + \frac{1}{2\pi i}\int\limits_{-\infty}^{0} d\omega' \frac{f^*_{\omega'}(t')f_{\omega'}(t)}{\omega-\omega'+i\epsilon}. \tag{2.4}$$

No further cuts from kinematic constraints on t are imposed in the determination of the eigenfuntions and eigenvalues. However, as we discuss in detail in Sec. 4, owing to the quasi-local nature of the BFKL kernel $\mathcal{K}$, this Green function is rapidly attenuated for large $|t-t'|$, which means that when it is inserted into the expression (2.1) in order to obtain the unintegrated gluon density, the diffusion into values of t substantially above the region of support of the impact factor $\Phi_p(t)$ is highly suppressed, thereby automatically limiting the gluon virtuality to be small compared with the incoming energy.

The infrared nonperturbative phases, η_n, which determine the values of the discrete eigenvalues, ω_n, are in general ω-dependent, but they must lie within a range of magnitude π, so that the quantum number n represents the number of oscillations of the eigenfunction between the scale t_0 at which the infrared phase condition is applied and the ultraviolet scale t_c at which the oscillatory behaviour becomes an exponentially decaying one. As pointed out in [4], an ω-dependent

*These phases should be universal (process-independent).

infrared phase condition is necessary in order to be able to express an impact factor with support only for small t in terms of the discrete eigenfunctions, since the frequency of oscillation of these eigenfunctions at small t is always below ~ 0.7. In fact, after imposing this nonperturbative phase, the eigenfunctions are forming an almost complete set of functions in the region of comparatively small $k \sim 1{-}10$ GeV.

The existence of this set of discrete eigenfunctions is consistent with the known fact that, in the Regge regime, the amplitude is determined by a set of Regge poles. The imposition of infrared phases does not in any way violate the kinematical constraint, but the ensuing discrete spectrum of eigenvalues has a very significant effect on the fitting of the results of this modified BFKL formalism to HERA data on the structure functions at low x.

The continuum contribution (for negative ω) is not significant for sufficiently small values of x at any given t. However, for a given x, as t increases these contributions become more significant and are essential in order for this formalism to match the double logarithmic limit of the DGLAP approach for sufficiently large t.

The value of t_c at which the oscillatory behaviour converts into an exponentially decaying one increases linearly with eigenvalue number n. For $n \gtrapprox 3$ this occurs at values of t_c above the scale at which one may expect to see physics beyond the Standard Model. The running of the coupling is therefore affected by the presence of thresholds for such a new physics and this in turn affects the positions of the discrete eigenvalues ω_n. For sufficiently low values of x the contribution from all but the first two or three eigenfunctions is negligible. However, we find that for values of x which are probed at HERA there is a sizable contribution from these higher eigenfunctions. This means that even though the transverse momenta do *not* diffuse into regions of t where the particles of new physics are actually produced, the shifts in the positions of the eigenvalues due to new physics affect the x-dependence of the unintegrated gluon density. Despite the fact that these effects are small, the high quality of the HERA data means that the quality of the fit is significantly affected by the possibility of new physics at high energies.

We now show how this works in detail.

2.1. LO Evaluation. We begin this subsection by reviewing the argument of [12] which led to a modification of the BFKL formalism which gives rise to discrete poles rather than a cut in the ω plane of the t-channel partial waves.

We consider the case of the leading-order BFKL equation [6] with running coupling also taken to leading order so that (for $t > 0$)

$$\bar{\alpha_s} \equiv \frac{C_A \alpha_s}{\pi} = \frac{1}{\bar{\beta}_0 t}, \tag{2.5}$$

where

$$\bar{\beta_0} \equiv \frac{\beta_0}{4C_A} = \frac{11}{12} - \frac{n_f}{18}. \tag{2.6}$$

The Hermitian BFKL kernel may be written as

$$\sqrt{\bar{\alpha_s}(t)\,\bar{\alpha_s}(t')}\mathcal{K}_0(t,t'),$$

where

$$\int dt' \mathcal{K}_0(t,t')\,\mathrm{e}^{i\nu t'} = \chi_0(\nu)\,\mathrm{e}^{i\nu t}, \tag{2.7}$$

$$\chi_0(\nu) = 2\Psi(1) - \Psi\left(\frac{1}{2} + i\nu\right) - \Psi\left(\frac{1}{2} - i\nu\right). \tag{2.8}$$

Note that the parameter ν may be real or imaginary for real eigenvalues $\chi_0(\nu)$.

The eigenfunctions $g_\omega(t)$ of this Hermitian kernel obey the eigenvalue equation

$$\int dt' \sqrt{\bar{\alpha_s}(t)\,\bar{\alpha_s}(t')}\,\mathcal{K}_0(t,t')\,g_\omega(t') = \omega g_\omega(t). \tag{2.9}$$

These eigenfunctions form a complete orthonormal set

$$\int dt g_\omega(t)\,g^*_{\omega'}(t) = 2\pi\delta(\omega - \omega'), \tag{2.10}$$

assuming (for the moment) a continuous spectrum for the eigenvalues ω.

They can be obtained by defining a set of functions $f_\omega(t)$:

$$f_\omega(t) = \frac{g_\omega(t)}{\sqrt{t}}, \tag{2.11}$$

which obey the eigenvalue equation

$$\bar{\alpha_s}(t) \int dt' \mathcal{K}_0(t,t') f_\omega(t') = \omega f_\omega(t). \tag{2.12}$$

Using Eq. (2.5), we have

$$\int dt' \mathcal{K}_0(t,t') f_\omega(t') = \bar{\beta}_0 \omega t f_\omega(t). \tag{2.13}$$

Taking the Fourier transform

$$f_\omega(t) = \int d\nu\,\mathrm{e}^{i\nu t}\,\tilde{f}_\omega(\nu) \tag{2.14}$$

and using Eq. (2.7), we have a first-order differential equation

$$\frac{d}{d\nu}\tilde{f}_\omega(\nu) = -\frac{i}{\bar{\beta}_0\omega}\chi_0(\nu)\tilde{f}_\omega(\nu), \tag{2.15}$$

which has a well-known solution

$$\tilde{f}_\omega(\nu) = \exp\left(-\frac{i}{\bar{\beta}_0\omega}\int^{\nu}\chi_0(\nu')d\nu'\right) = \left[\frac{\Gamma(1/2+i\nu)}{\Gamma(1/2-i\nu)}\,\mathrm{e}^{-2i\Psi(1)\nu}\right]^{1/(\bar{\beta}_0\omega)}. \tag{2.16}$$

In this way we obtain

$$f_\omega(t) = \frac{1}{\sqrt{2\pi\omega}}\int_{-\infty}^{+\infty} d\nu\,\mathrm{e}^{i\nu t}\left[\frac{\Gamma(1/2+i\nu)}{\Gamma(1/2-i\nu)}\,\mathrm{e}^{-2i\Psi(1)\nu}\right]^{1/(\bar{\beta}_0\omega)}, \tag{2.17}$$

where the prefactor is taken such that the normalization condition (2.10) is obeyed.

The integral over ν can be performed numerically over a suitable contour. A very good approximation to this integral (for small ω) is obtained by the saddle-point approximation (equivalent to solving Eq. (2.13) using the semiclassical approximation). The saddle point, which is a function of t, $\nu_s(t)$, is obtained from the solution to

$$\chi_0\left(\nu_s(t)\right) = \bar{\beta}_0\omega t. \tag{2.18}$$

We consider two regions depending on whether t is greater or less than a critical point, t_c, given by

$$\bar{\beta}_0\omega t_c = \chi_0(0) = 4\ln 2. \tag{2.19}$$

2.1.1. $t > t_c$. In this case there is a single saddle point on the positive imaginary axis, shown in Fig. 1. If we define γ_s by

$$\gamma_s = \frac{1}{2} + i\nu_s, \tag{2.20}$$

then at the saddle point, γ_s, is the solution to

$$\chi_0(\gamma_s) \equiv 2\Psi(1) - \Psi(\gamma_s) - \Psi(1-\gamma_s) = \\ = \bar{\beta}_0\omega t, \tag{2.21}$$

γ_s is in the range

$$0 < \gamma_s < \frac{1}{2}.$$

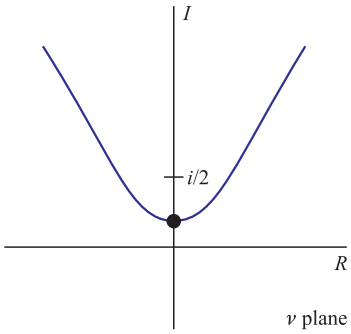

Fig. 1. (Color online) Integration contour (blue line) on the ν plane for $t > t_c$. The black dot shows the position of the saddle point, ν_s

The contour of integration is deformed so that it becomes the contour of steepest descent obtained from the solution to

$$\arg\left\{\int_{\nu_s}^{\nu}\chi(\nu')d\nu' - \chi(\nu_s)\,(\nu-\nu_s)\right\} = -\frac{\pi}{2}.$$

Near the saddle point the contour runs parallel to the real axis, but for very large $|\nu|$ it runs parallel to the imaginary axis. In the saddle-point approximation, we obtain (using Eq. (2.21))

$$f_\omega(t) = \sqrt{\frac{1}{2\chi_0'(\gamma_s)}}\, \mathrm{e}^{-t/2}\, \mathrm{e}^{\gamma_s t} \left[\mathrm{e}^{(\gamma_s - 1/2)\Psi(1)} \frac{\Gamma(\gamma_s)}{\Gamma(1-\gamma_s)} \right]^{1/(\bar{\beta}_0 \omega)}. \tag{2.22}$$

This is an exponentially decreasing function of t. Moreover, γ_s can be related to the anomalous dimension in the DGLAP formalism, since

$$\frac{d}{dt}\left(\mathrm{e}^{t/2} f_\omega(t) \right) = \gamma_s \left(\mathrm{e}^{t/2} f_\omega(t) \right). \tag{2.23}$$

From Eq. (2.18), the anomalous dimension is

$$\gamma_s \;\approx\; \frac{\bar{\alpha_s}(t)}{\omega} + O\left(\frac{\bar{\alpha_s}(t)^2}{\omega^2} \right),$$

in agreement with DGLAP for small γ_s.

2.1.2. $t < t_c$. Here we have two saddle points lying on the real axis at $\pm\nu_s$, shown in Fig. 2. The positions of the saddle points are obtained from

$$2\Psi(1) - 2\,\mathrm{Re}\left\{ \Psi\left(\frac{1}{2} + i\nu_s \right) \right\} = \bar{\beta}_0 \omega t. \tag{2.24}$$

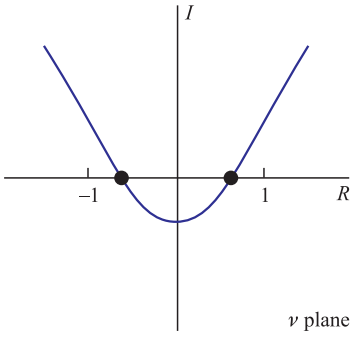

Fig. 2. (Color online) Integration contour (blue line) on the ν plane for $t < t_c$. The black dots show the positions of the saddle points, $\pm|\nu_s|$

We need to integrate around both of these saddle points, taking a contour of steepest descent in the vicinity of the saddle points, which in this case is inclined at an angle of $\pm\pi/4$ to the real axis and enclose the positive imaginary axis at large ν. The saddle-point approximation then yields

$$f_\omega(t) = \sqrt{\frac{2}{\chi'(\nu_s)}} \sin\left(\nu_s t + \frac{\phi(\nu_s)}{\bar{\beta}_0 \omega} + \frac{\pi}{4} \right), \tag{2.25}$$

where

$$\phi(\nu_s) = \arg\left\{ \mathrm{e}^{-2i\Psi(1)\nu_s} \frac{\Gamma(1/2 + i\nu_s)}{\Gamma(1/2 - i\nu_s)} \right\}. \tag{2.26}$$

The inclusion of $\pi/4$ in the phase in Eq. (2.25) ensures a matching of the solutions at $t = t_c$. Near $t = t_c$ the solution is given by an Airy function.

For $t < t_c$, we have an oscillatory solution which does *not* lend itself to a match to the DGLAP formalism — in this regime a DGLAP analysis is *not*

appropriate, since in this region the saddle point γ_s is complex and double-valued, i.e.,

$$\gamma_s = \frac{1}{2} \pm i|\nu_s|,$$

and cannot be related to the (real) anomalous dimension of the DGLAP formalism. In this region the DGLAP equation is not valid and the BFKL equation can be considered as a generalized (quantized) version of the DGLAP equation.

Recall that the saddle point, $\nu_s(t)$, is a function of t and so we do not have constant frequency oscillations. As $t \to 0$, ν_s tends to a value $\nu_0 \approx 0.635$ and we have constant frequency oscillations in the infrared limit. As t increases, this frequency decreases, becoming zero at $t = t_c$.

The infrared phase at $t = 0$, calculated from perturbative QCD (with $t > 0$), is then given by

$$\eta_0 \pi = \frac{\phi(\nu_0)}{\bar{\beta}_0 \omega} + \frac{\pi}{4} \tag{2.27}$$

($\phi(\nu_0) \approx 0.96$). This phase is only determined up to a multiple of π. We now make a very general assumption that the infrared properties of QCD fixe this phase (in general as a function of ω) to be $\eta(\omega)$, where the function $\eta(\omega)$ is determined from the nonperturbative regime of QCD ($t \leqslant 0$). The matching of the two phases η_0 and $\eta(\omega)$ in the semiclassical solution, Eq. (2.25), then restricts the allowed values of ω to a discrete set ω_n that satisfy the equation

$$\frac{\phi(\nu_0)}{\pi \bar{\beta}_0 \omega_n} = \eta(\omega_n) + \left(n - \frac{1}{4}\right) \quad (n = 1, 2, 3, \ldots) \tag{2.28}$$

The function $\eta(\omega)$ could be a constant (as originally proposed in [12]), but in general it can vary with ω. Because of periodicity it can take values in the interval between 0.25 and -0.75 only. Although $\eta(\omega)$ cannot be determined from the perturbative analysis described here, its restricted range limits its effect on the determination of the eigenvalues (see Subsec. 2.5). However, its variation with ω is very important in the construction of the gluon density (see Sec. 3).

The above analysis shows clearly that the solution of the BFKL equation has to be given by the set of discrete eigenfunctions, whose support in the virtual gluon transverse momentum is determined by the critical point, t_c, Eq. (2.19), and whose phase $\eta(\omega)$ at some low transverse momentum is determined by the nonperturbative sector of QCD. Effectively, the boundary conditions modify the BFKL kernel so that it may be written as

$$\mathcal{K}(t, t') = \sum_n \omega_n f_n^*(t) f_n(t'). \tag{2.29}$$

This coincides with the (LO) kernel

$$\bar{\alpha_s}(t) K_0(t, t'),$$

provided it acts on a function $f(t)$ which may be written as a superposition of the eigenfunctions $f_n(t)$:

$$f(t) = \sum_n a_n f_n(t).$$

In this way we have supplemented the kernel with both infrared and ultraviolet boundary conditions. The infrared boundary conditions arise from the nonperturbative sector of QCD, but the ultraviolet boundary conditions arise naturally from the asymptotic freedom of QCD. Importantly, the behaviour of the eigenfunctions in the ultraviolet is controlled by a critical value, t_c, of transverse momentum, which grows almost linearly with n in accordance with the fact that the period of oscillations is practically independent of n. Therefore, the n-dependent boundary condition leads to qualitatively different results from those obtained using a kernel in which boundary conditions are effected simply by a cutoff on a wave function.

Furthermore, we note that the value of this critical transverse momentum depends almost entirely on the eigenvalue ω, which decreases like $1/n$, for large n, as the quantum number n increases (see Eq. (2.28)). This means that in turn the value of the critical transverse momenta k_c increases exponentially as ω decreases, so that the nth critical momentum is given by (inserting Eq. (2.28) into Eq. (2.19))

$$k_c^{(n)} = \Lambda_{\rm QCD} \exp\left\{ \frac{2\pi \ln 2}{\phi(\nu_0)} \left(n - \frac{1}{4} + \eta(\omega_n) \right) \right\} \approx \Lambda_{\rm QCD}\, {\rm e}^{4.5\, n}. \qquad (2.30)$$

Finally, let us note that our solution of the BFKL equation is similar to the WKB method for the bound-state solution of the Schrödinger equation in the semiclassical approximation; the critical point, t_c, is analogous to the turning point x_c where the potential is equal to the energy. Inside a potential well the solutions are oscillatory and outside they decay exponentially. This shows that the solution of the BFKL equation (1.1) consists of the superposition of the bound-state eigenfunctions of the two gluon system with pseudo-energies given by the eigenvalues ω_n. Knowledge of the eigenvalues gives important information about the interactions between gluons, in both the infrared and ultraviolet regions of k. We note that in the solution of the BFKL equation, the oscillations of the eigenfunctions at large k should cancel each other in accordance with the kinematical constraints provided by the beam energy of the experiment. This imposes additional restrictions on the nonperturbative phases $\eta(\omega)$ (see below).

2.2. Threshold Effects. The above analysis assumes that $\bar{\beta}_0$ is a constant, so that the coupling $\bar{\alpha_s}(t)$ is given simply by Eq. (2.5). However, we know that there are thresholds at $t = t_i$ where heavy flavour quarks can be produced, and also there may be extra thresholds arising from BSM physics with a threshold (that according to Eq. (2.30) can be large) below $t = t_c$. This means that Eq. (2.17) can only be used as a solution for $f_\omega(t)$ between thresholds. As an example, suppose

that there is only one threshold, at $t = t_t$ below the critical point, t_c, and that $\bar{\beta}_0$ takes the value $\bar{\beta}_0{}^{>}$ above this threshold and $\bar{\beta}_0{}^{<}$ below. At $t \geqslant t_t$ we have

$$f_\omega(t) = \frac{1}{\sqrt{2\pi\bar{\beta}_0\omega}} \int d\nu\, \mathrm{e}^{i\nu t} \left[\frac{\Gamma(1/2+i\nu)}{\Gamma(1/2-i\nu)}\, \mathrm{e}^{-2i\Psi(1)\nu}\right]^{1/(\bar{\beta}_0{}^{>}\omega)} \tag{2.31}$$

and for $t < t_t$ we have

$$f_\omega(t) = A \int d\nu\, \mathrm{e}^{i\nu t} \left[\frac{\Gamma(1/2+i\nu)}{\Gamma(1/2-i\nu)}\, \mathrm{e}^{-2i\Psi(1)\nu}\right]^{1/(\bar{\beta}_0{}^{<}\omega)} f_\omega(t_t), \tag{2.32}$$

with the constant A chosen to be

$$A^{-1} = \int d\nu\, \mathrm{e}^{i\nu t_t} \left[\frac{\Gamma(1/2+i\nu)}{\Gamma(1/2-i\nu)}\, \mathrm{e}^{-2i\Psi(1)\nu}\right]^{1/(\bar{\beta}_0{}^{<}\omega)}, \tag{2.33}$$

so that the solutions match at $t = t_t$.

In the saddle-point approximation, we can handle such thresholds by noting that Eq. (2.17) can be written as

$$f_\omega(t) = \frac{1}{\sqrt{2\pi\omega}} \int d\nu\, \mathrm{e}^{iS(\nu,t)/\omega}, \tag{2.34}$$

where the «action» $S(\nu, t)$ is given by

$$S(\nu, t) = \omega\nu t - \frac{1}{\bar{\beta}_0} \int_0^\nu \chi_0(\nu')\, d\nu'. \tag{2.35}$$

At the saddle point $\nu = \nu_s(t)$, upon integrating by parts this may be rewritten as

$$S(t) = \omega \int_{t_c}^{t} \nu_s(t')\, dt', \tag{2.36}$$

where the function $\nu_s(t)$ is given by Eq. (2.18). (We have used the notation $S(t)$ to denote $S(\nu_s(t), t)$ — it is now a function of t only.) Here we see explicitly that the saddle-point approximation for integral (2.34) is equivalent to the semiclassical approximation. Replacing the integral over ν in Eq. (2.34) by the value of the integrand at the saddle point, we obtain a solution which obeys the differential equation

$$\frac{d}{dt} f_\omega(t) = \chi^{-1}(\bar{\beta}_0\omega t)\, f_\omega(t). \tag{2.37}$$

The semiclassical approximation consists of the assumption that the solution to Eq. (2.13) is the solution to Eq. (2.37) multiplied by a slowly varying factor, which turns out to be the same as that obtained in the Gaussian integral around the saddle point in Eq. (2.34). In analogy with the WKB approximation in the Schrödinger equation there exists a critical point, t_c, at which the approximate solution changes from an oscillatory function to an exponentially decaying one. The assumption of a slowly varying prefactor breaks down at this point, but the solutions on either side of the critical point can be matched using a suitable Airy function. It is this matching, together with some property of the behaviour at $t = 0$, that determines the allowed eigenvalues.

Thresholds are handled in general by replacing Eq. (2.18) by the more general relation

$$\chi_0\left(\nu_s(t)\right) = \frac{\omega}{\bar{\alpha_s}(t)}. \tag{2.38}$$

$\bar{\alpha_s}(t)$ may now be determined using the β function with appropriate thresholds.

The eigenfunctions for $t \ll t_c$ now take the form

$$f_\omega(t) = \frac{C}{\sqrt{\chi_0'(\nu_s(t))}} \sin\left(\frac{S(t)}{\omega} + \frac{\pi}{4}\right) \tag{2.39}$$

and the semiclassical quantization condition on the allowed eigenvalues becomes

$$\frac{S(0)}{\omega_n} = \left(\eta(\omega_n) + n - \frac{1}{4}\right)\pi. \tag{2.40}$$

Comparing this with Eq. (2.28), we see that $S(0)$ is independent of ω^*. However, its value clearly depends on the positions of the thresholds in $\bar{\beta_0}$, Eqs. (2.31) and (2.32). Already for $n \geqslant 3$ the value of k_c given by Eq. (2.30) exceeds many tens of TeV, and this means that the spectrum is sensitive to any BSM physics. The BSM effect changes the perturbative phase η if the corresponding threshold, k_t, is below the critical point, $k_c^{(n)}$. The effect of such a threshold can be readily estimated; let us assume that for a given eigenvalue ω, the threshold $t_t \equiv \ln\left(k_t^2/\Lambda_{\mathrm{QCD}}^2\right)$ is the largest threshold, below the critical point t_c, and that in the range

$$t_t < t < t_c,$$

$\bar{\beta_0}$ takes the value $\bar{\beta_0}^>$. The exact solution for the LO BFKL with running coupling at $t = t_t$ is

$$f(t_t) \propto \int d\nu\, \mathrm{e}^{i\phi(\nu, t_t)}, \tag{2.41}$$

*For sufficiently large n we can see this directly since $S(0) \sim \mathcal{O}(\omega_n t_c^{(n)})$ and whereas $t_c^{(n)} \propto n$, $\omega_n \propto 1/n$.

where

$$\phi(\nu, t_t) = \nu\left(t_t - 2\frac{\Psi(1)}{\bar{\beta}_0{}^{>}\omega}\right) + \frac{2}{\bar{\beta}_0{}^{>}\omega}\arg\left\{\Gamma\left(\frac{1}{2} + i\nu\right)\right\}. \tag{2.42}$$

We evaluate this integral using the saddle-point method and assuming that the threshold occurs sufficiently close to the critical point t_c, that ν_s is sufficiently small for the diffusion approximation to be valid. The phase difference between the case where there is a threshold at $t = t_t$ and the case where there is no threshold is then

$$\Delta\phi = \frac{2}{3\omega\sqrt{14\zeta(3)}}\left[\frac{1}{\bar{\beta}_0{}^{<}}\left(4\ln 2 - \bar{\beta}_0{}^{<}\omega t_t\right)^{3/2} - \right.$$
$$\left. - \frac{1}{\bar{\beta}_0{}^{>}}\left(4\ln 2 - \bar{\beta}_0{}^{>}\omega t_t\right)^{3/2}\right], \tag{2.43}$$

where $\bar{\beta}_0{}^{<}$ denotes the value of $\bar{\beta}_0$ below the threshold.

We observe that the above phase difference is substantial for $\omega \leqslant 0.1$ and that this difference is not suppressed by the scale of the BSM physics. In this sense our analysis differs fundamentally from the treatment of the Standard Model as a low-energy effective theory way below the thresholds of new physics. In the latter case, logarithmic corrections can always be absorbed into unphysical renormalization constants of the renormalizable operators of the effective theory, leaving only higher dimension operators whose coefficients are suppressed by powers of the new-physics mass scale.

2.3. NLO Evaluation. We have shown in [4] that the BFKL integral equation can be cast in the form of the pseudo-differential equation

$$\bar{\alpha_s}(t)\int dt' \mathcal{K}_0(t,t') f_\omega(t') = \chi\left(-i\frac{d}{dt}, \alpha_s(t)\right) f_\omega(t) = \omega f_\omega(t). \tag{2.44}$$

Making the simplifying assumption that $\bar{\alpha_s}$ is given by Eq. (2.5) and taking into account the collinear resummation [10], we can write the BFKL equation in the next-to-leading order as

$$\bar{\beta}_0\omega t f_\omega(t) = \left[\tilde{\chi}_0(\hat{\nu}, \omega) + \frac{1}{t\bar{\beta}_0}\xi(\hat{\nu})\right] f_\omega(t), \tag{2.45}$$

where the operator $\hat{\nu} = -id/dt$,

$$\tilde{\chi}_0(\nu, \omega) = 2\Psi(1) - \Psi\left(\frac{1}{2} + i\nu + \frac{\omega}{2}\right) - \Psi\left(\frac{1}{2} - i\nu + \frac{\omega}{2}\right)$$

and

$$\xi(\nu) = \chi_1(\nu) + \frac{1}{2}\left[2\Psi(1) - \Psi\left(\frac{1}{2} + i\nu\right) - \Psi\left(\frac{1}{2} - i\nu\right)\right] \times$$
$$\times \left[\Psi'\left(\frac{1}{2} + i\nu\right) + \Psi'\left(\frac{1}{2} - i\nu\right)\right],$$

where χ_1 denotes the NLO characteristic function [9]. The function $\xi(\nu)$ does not have the poles of the third order of the form $\sim 1/(1/2 \pm i\nu)^3$, in agreement with a renormlaization group analysis [9].

Equation (2.45) can be considered as a quadratic equation in t:

$$[\omega(t\bar{\beta}_0)^2 - t\bar{\beta}_0\tilde{\chi}_0(\hat{\nu},\omega) - \xi(\hat{\nu})]\, f_\omega(t) = 0. \tag{2.46}$$

We can convert this into a second-order differential equation for the Fourier transform $\tilde{f}_\omega(\nu)$, where t is replaced by the operator $\hat{t} = i(d/d\nu)$. In the semiclassical approximation in which $\ln(\chi_0)$ and $\ln(\xi)$ are treated as slowly varying functions of ν, so that

$$\hat{t}^2\tilde{f}_\omega \approx \left(\hat{t}(\ln\, \tilde{f}_\omega)\right)^2 \tilde{f}_\omega,$$

this second-order differential equation may be written as

$$\left[i\bar{\beta}_0\hat{t} - X^-(\nu,\omega)\right]\left[i\bar{\beta}_0\hat{t} - X^+(\nu,\omega)\right]\, \tilde{f}_\omega(\nu) = 0, \tag{2.47}$$

where

$$X^\pm(\nu,\omega) = \frac{1}{2\omega}\tilde{\chi}_0(\nu,\omega) \pm \sqrt{\left(\frac{1}{2\omega}\right)^2 \tilde{\chi}_0(\nu,\omega) + \frac{1}{\omega}\xi(\nu)},$$

with solution for $f_\omega(t)$ which is analogous to the LO expressions of Eqs. (2.14) and (2.16):

$$f_\omega(t) = \int\limits_{-\infty}^{\infty} d\nu\, \mathrm{e}^{i\nu t} \exp\left(-\frac{i}{\bar{\beta}_0}\int^{\nu} X^+(\nu,\omega)\, d\nu\right). \tag{2.48}$$

For small ω, Eq. (2.48) may be approximated by

$$f_\omega(t) = \frac{1}{\sqrt{2\pi\omega}} \int\limits_{-\infty}^{+\infty} d\nu\, \mathrm{e}^{i\nu t}\left[\frac{\Gamma(1/2+i\nu)}{\Gamma(1/2-i\nu)}\, \mathrm{e}^{-2i\Psi(1)\nu}\right]^{1/(\bar{\beta}_0\omega)} \times$$

$$\times \exp\left[-\frac{i}{\bar{\beta}_0{}^2\omega t}\int^{\nu} d\nu'\, \xi(\nu')\right]. \tag{2.49}$$

Note that the saddle point of the integral over ν in Eq. (2.49) occurs at ν_s where the RHS of Eq. (2.45) vanishes as required for $\tilde{f}_\omega(\nu_s)$ to be a turning point.

In a more general NLO approach, the BFKL Eq. (2.44) can be simplified using the semiclassical approximation, i.e., assuming that the t-dependence of $\ln\, f_\omega(t)$ is large so that

$$\left(\frac{d}{dt}\right)^r f_\omega(t) \approx f_\omega(t)\left(\frac{d\ln f_\omega(t)}{dt}\right)^r. \tag{2.50}$$

Equation (2.44) looks then like the nonlinear differential equation

$$\chi\left(-i\frac{d\ln f_\omega(t)}{dt},\alpha_s(t)\right)=\chi(\nu(t),\alpha_s(t))=\omega. \tag{2.51}$$

As a result, the frequency $\nu(t)$ is a function of t such that

$$\omega=\left(\frac{\alpha_s(t)C_A}{\pi}\right)\chi_0(\nu)+\left(\frac{\alpha_s(t)C_A}{\pi}\right)^2\chi_1(\nu)+\dots \tag{2.52}$$

The expression (2.52), including collinear resummation [10], is the NLO analog of Eq. (2.38). Equation (2.51) has a solution

$$f_\omega(t)=\mathrm{e}^{iS(t)/\omega}, \tag{2.53}$$

where

$$S(t)=\omega\int\limits_{t_c}^{t}\nu(t')\,dt'. \tag{2.54}$$

The critical logarithmic transverse momentum, t_c, is the value of t for which $\nu(t)=0$. This condition is the NLO analog of Eq. (2.19). For $t<t_c$, there are two real solutions for $\nu(t)$ generating an oscillatory solution with a given phase, whereas for $t>t_c$ the solution is on a positive imaginary axis, generating an exponentially decaying function as $t\to\infty$.

Thus, we see that the solution for the eigenfunctions in semiclassical approximation is analogous to that in leading order, but the function $\nu(t)$ takes into account the NLO characteristic function as well as the NLO running of the coupling and the threshold effects. A further feature of threshold effects beyond leading order is that it is not only the β function that has steps at the thresholds but also the NLO contributions to the characteristic function $\delta\chi_1$, corresponding to the presence of new particles at some point in the ladders [14].

The semiclassical approximation is valid provided

$$\frac{d\ln(\nu(t))}{dt}\ll\nu(t).$$

This condition breaks down in the region $t\sim t_c$ where $|\nu(t)|$ is very small. However, in this region the eigenvalue equation approximates to Airy's equation with solution

$$f_\omega(t)=\mathrm{Ai}\left(\left(\frac{3}{2}\frac{S(t)}{\omega}\right)^{2/3}\right), \tag{2.55}$$

For $t\gg t_c$ the Airy function, Ai, behaves as

$$\mathrm{Ai}\left(\left(\frac{3}{2}\frac{S(t)}{\omega}\right)^{2/3}\right)\sim\mathrm{e}^{-|S(t)|/\omega}, \tag{2.56}$$

and for $t \ll t_c$

$$\mathrm{Ai}\left(\left(\frac{3}{2}\frac{S(t)}{\omega}\right)^{2/3}\right) \sim \sin\left(\frac{S(t)}{\omega}+\frac{\pi}{4}\right). \tag{2.57}$$

We therefore find that the solution of Eq. (2.55) is a good approximation over the entire range of t and at the same time determines the phase of the oscillatory solution for $t = t_c$ required to match the oscillatory region and the exponentially decaying region. As in the LO case, we make a very general assumption that the infrared (nonperturbative) properties of QCD impose some phase, η at $t = 0$, defined up to an ambiguity of $n\pi$, which can also depend on ω. We find then that we can only match this phase to the perturbative one, determined from Eq. (2.54), for one value of ω for each integer n, where n corresponds to the number of oscillations. This leads to the quantization of the spectrum (i.e., discrete pomeron poles) given by Eq. (2.40), in keeping with the predictions of Regge theory.

In contrast to the LO evaluation, in full NLO the eigenvalues and eigenfunctions can only be determined using numerical methods of iteration and integration. Their construction requires several steps; in the first step we determine the values of the frequency ν as a function of ω and t from the solutions of Eq. (2.52). Then, the critical point, t_c, is determined as a function of ω from the condition $\nu(t_c) = 0$. The phase function $S(t)$, for a given ω, is then found from Eq. (2.54).

In the next step the phase η at the infrared boundary has to be specified. In the leading-order computation it was possible to define it at Λ_{QCD}, because the frequency ν is well defined at $t = 0$, Eq. (2.18). For the NLO calculation, we obtain ν with the help of Eq. (2.52), which is not valid at Λ_{QCD}. We therefore defined it as a phase condition at the lowest possible value of the (logarithmic) transverse momentum, $t = t_0$, which can be safely reached by the perturbative calculation (see also the discussion in Subsec. 3.2).

2.4. $N = 1$ **Supersymmetry at Various Thresholds.** We have chosen as example of «new physics» the popular $N = 1$ supersymmetric extension of the Standard Model above a given threshold in k_T, which for simplicity we assume to be a common mass threshold for all superpartners. Below this threshold the running of the coupling is governed by the β function to two-loop order

$$\beta_< = -\frac{\alpha_s^2}{4\pi}\left(\frac{11C_A}{3}-\frac{2}{3}n_f\right) - \frac{\alpha_s^3}{(4\pi)^2}\left(\frac{34C_A^2}{3}+\left(\frac{10C_A}{3}+2C_F\right)n_f\right), \tag{2.58}$$

where for the case of QCD, $C_A = 3$, $C_F = 4/3$ and n_f is the number of active flavours. Above the threshold, the beta function is given by

$$\beta_> = -\frac{\alpha_s^2}{4\pi}\left(3C_A - n_f\right) - \frac{\alpha_s^3}{(4\pi)^2}\left(6C_A^2+\left(-\frac{2C_A}{3}+2C_F\right)n_f\right). \tag{2.59}$$

This leads to a «kink» (discontinuity in the derivative) in the running of α_s at the threshold for $N = 1$ SUSY, which can be seen in Fig. 3.

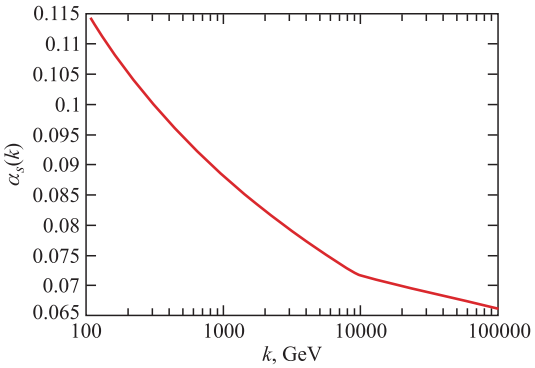

Fig. 3. The running of α_s across a threshold for $N = 1$ SUSY at 10 TeV

Furthermore, above the SUSY threshold, the NLO characteristic function $\chi_1(\nu)$ acquires an additional contribution [14] of

$$\delta_f \chi_1(\nu) = \frac{\pi^2}{32} \times \\ \times \frac{\sinh(\pi\nu)}{\nu(1+\nu^2)\cosh^2(\pi\nu)} \left(\frac{11}{4} + 3\nu^2\right) \quad (2.60)$$

from the octet of Majorana fermions (gluinos), and

$$\delta_s \chi_1(\nu) = -\frac{\pi^2}{32} \times \\ \times \frac{n_f}{C_A^3} \frac{\sinh(\pi\nu)}{\nu(1+\nu^2)\cosh^2(\pi\nu)} \left(\frac{5}{4} + \nu^2\right) \quad (2.61)$$

from the squarks (in the fundamental representation).

Typical graphs contributing to $\delta_s \chi_1(\nu)$ are shown in Fig. 4. They contribute only at NLO level since the exchange of a fermion or scalar particle in the t-channel is suppressed in LLA [9], and therefore only contributes at subleading logarithm order.

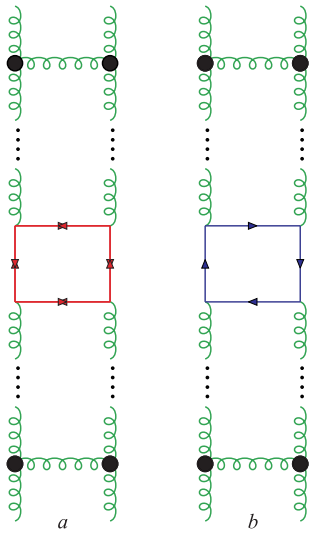

Fig. 4. Typical graphs contributing to BFKL kernel involving gluinos (a) or squarks (b)

2.5. The Discrete Pomeron with and without SUSY. In this subsection we investigate the properties of the discrete BFKL pomeron with and without SUSY contributions. For this example, we have assumed that the SUSY threshold is at 10 TeV. Figure 5 shows the spectrum of the eigenvalues ω_n computed in the NLO computation assuming that the nonperturbative phase $\eta(\omega_n)$ of the eigenvalue condition, Eq. (2.40), is $\eta = -0.25$, for all eigenfunctions. The per-

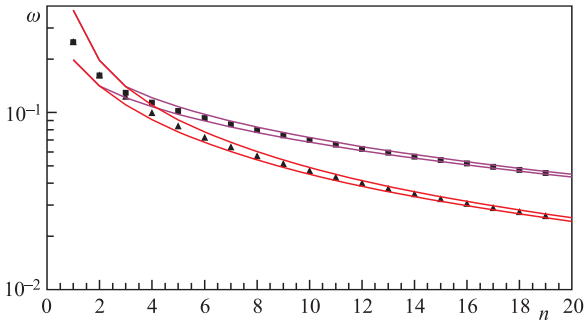

Fig. 5. The eigenvalues computed in the NLO evaluation of the Standard Model (triangles) and SUSY at a threshold of 10 TeV (squares). The lines indicate the maximal possible spread due to the uncertainty of the phase (η) choice

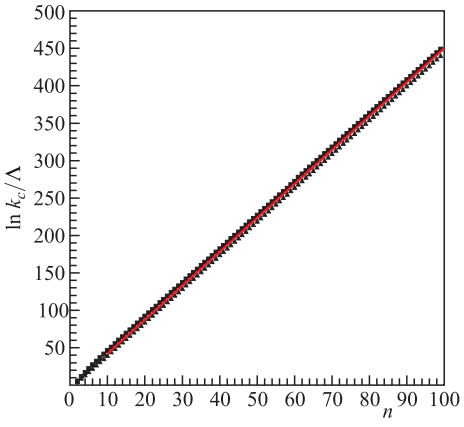

Fig. 6. (Color online) The critical point k_c computed in the NLO evaluation of the Standard Model (triangles) and SUSY at a threshold of 10 TeV (squares). The red lines show the LO computation which is not sensitive to any threshold effects

turbative phase, $S(0)$ of Eq. (2.40), at the infrared boundary $t = 0$, is replaced by $S(k_0)$, with $k_0 = \Lambda_{\rm QCD} \exp(t_0/2)$ and $k_0 = 0.6$ GeV. The eigenvalues determined with and without SUSY effects differ substantially for $n \geqslant 3$, whereas for $n < 3$ they show no difference. This is understandable from the Appelquist–Carrazone theorem [7], because the assumed SUSY threshold that we have chosen lies between the critical momenta for the second eigenfunction ($k_c \sim 1$ TeV) and the third eigenfunction ($k_c \sim 100$ TeV). The k_c values computed at NLO, with and without the SUSY threshold, are shown in Fig. 6. They turn out to be very close to the leading-order values calculated from Eq. (2.30) — the difference being due to the fact that α_s runs more rapidly for NLO than for LO. Furthermore, these critical momenta show only small dependence on the presence on SUSY threshold.

On the other hand, the eigenvalues ω_n, which are important for the description of the HERA structure-function data at low x, are very sensitive to possible threshold effects; i.e., they differ substantially already in LO and the differences are much larger than any possible uncertainties due to the unknown phase η.

For example, in LO, Eq. (2.28), the ratio of $\bar{\beta}_0$'s below and above the SUSY threshold is 7/3, which means that already for $n \geqslant 3$ the effect of the change in $\bar{\beta}_0$ on the eigenvalues is much larger than the maximal possible effects due to the uncertainty in η (η can only vary between $\eta = 0.25$ and $\eta = -0.75$). At NLO, we find that the phase-independent discrepancy between the eigenvalues with and without the SUSY threshold starts at $n \geqslant 5$ (see Fig. 5). These substantial differences are related to the fact that for $\omega < 0.1$ the change of phase of an eigenvalue, $\Delta\phi$, arising from the change in $\bar{\beta}_0$ as one crosses the SUSY threshold is large (as can be seen from Eq. (2.43)) and indeed much larger than the maximal possible η change, $\Delta\eta \leqslant 1$.

Since the properties of the eigenvalues are determined by the behaviour at very high virtualities (of the order of k_c), it should be expected that the eigenvalues computed in NLO should approach the LO ones at large n^*. Figure 7 shows the comparison of the eigenvalues computed using the NLO and LO approximations and confirms this expectation. The LO computation was made using Eq. (2.28) with $\bar{\beta}_0$ values computed with $n_f = 6$ below the SUSY threshold of 10 TeV. It is interesting to observe that LO and NLO results approach each other more slowly in the case of the SM+SUSY than in the SM alone. This slower approach is due to the fact that α_s runs more slowly above the SUSY threshold. This means that the eigenvalues ω_n approach zero at a different pace, as can be seen from the figure. We note that for small ω, the eigenvalues are very closely packed and so the effect of the discrete nature of the solutions becomes less important. To a good approximation we could replace the sum over the eigenfunctions for small ω by an integral over a range of small ω. However, it is important to

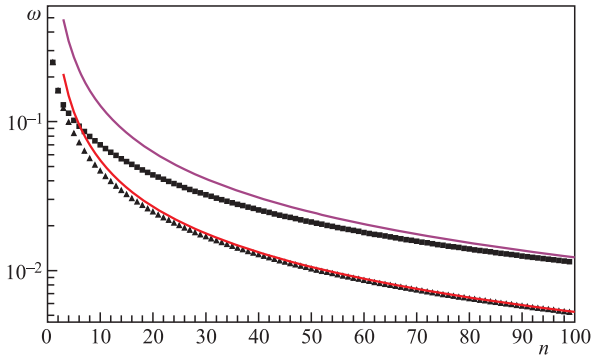

Fig. 7. The eigenvalues computed in the NLO evaluation of the Standard Model (triangles) and SUSY at a threshold of 10 TeV (squares). The lines show the LO computation in the two cases

*For sufficiently small ω, the NLO effects both in $\bar{\beta}_0$ and in the characteristic function χ become negligible.

note that the Jacobian for the transition from a discrete sum to an integral is proportional to the gradient of the $\omega - n$ distribution shown in Fig. 7, and this is different in the two cases — leading to different pomeron amplitudes.

In addition to the change of the running of α_s, there are also effects due to the $\delta\chi_1$ contributions to χ_1 which sets in above the SUSY threshold, Eqs. (2.60) and (2.61). It is this discontinuity which is responsible for the discontinuities in the frequencies ν at threshold, see Fig. 8, and *not* the change in the rate of running of the coupling, which remains a continuous function*. The change in frequency thus compensates for the change in the characteristic function in order to ensure that the eigenvalues ω_n remain unchanged as one passes through the

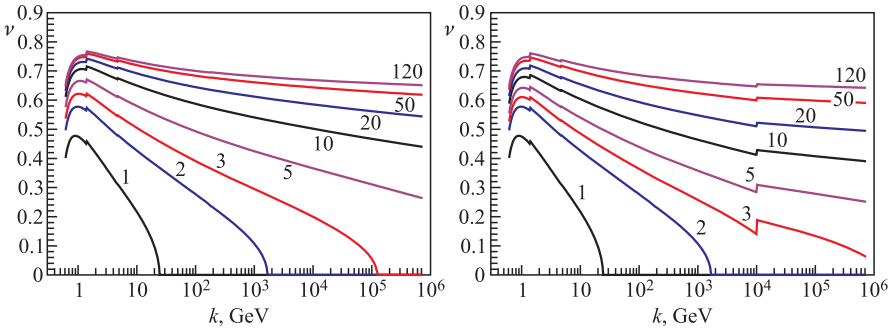

Fig. 8. Oscillation frequencies as a function of gluon transverse momentum for various eigenfunctions. The left-hand panel is the case of the Standard Model and the right-hand panel is the case of $N = 1$ SUSY above a threshold of 10 TeV. For the purpose of this comparison, it has been assumed that the infrared phases are the same in both cases

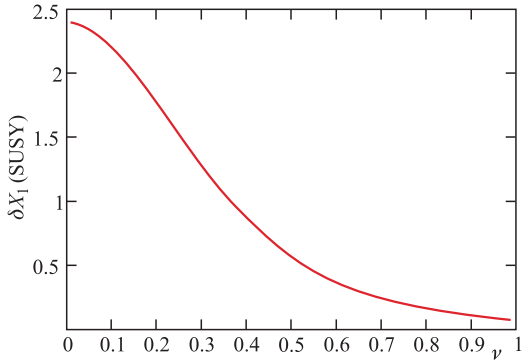

Fig. 9. Decrease in the NLO characteristic function χ_1 as a function of frequency ν

*A similar smaller discontinuity can be seen at around 3 GeV. This corresponds to the c-quark threshold. There are analogous, even smaller, discontinuities at the b-quark and t-quark thresholds.

threshold*. The contribution, $\delta\chi_1$, of these additional terms is shown as a function of frequency in Fig. 9, where it can be seen that this is a rapidly decreasing function, which explains why the discontinuities in frequency at threshold are much larger for the lower eigenfunctions for which the frequency at threshold is lower.

For lower n eigenfunctions, the change of the frequencies due to the SUSY threshold leads also to the change of its shape. In Fig. 10 we show a representative

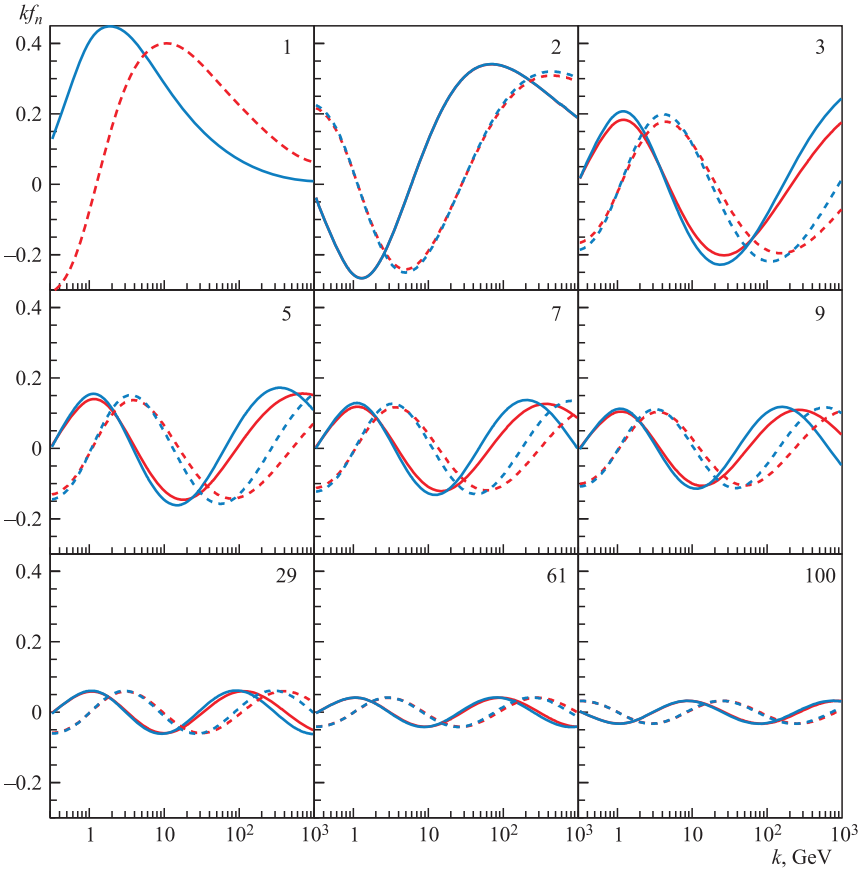

Fig. 10. (Color online) Comparison of a representative subset of eigenfunctions in the Standard Model (blue) and the SUSY model (red) computed at $\eta = -0.25$ (solid line) and $\eta = +0.25$ (dashed line). The SUSY threshold is assumed at 10 TeV. The eigenvalue number is given in the upper right corner

*The discontinuous changes in frequency are due to the fact that the change in characteristic function is imposed at a threshold in its entirety. A determination of the NLO characteristic function which accounted for the mass of internal particles would smooth out these discontinuities.

subset of eigenfunctions in the Standard Model and the SUSY model in the transverse momentum region relevant for a fit to HERA data. The eigenfunctions are shown with values of $\eta = -0.25$ and $\eta = +0.25$ (in order to give an indication of the sensitivity of the allowed eigenvalues to the unknown infrared phases), with and without SUSY at a threshold of 10 TeV. As expected, the first two eigenfunctions are identical since their values of k_c are below the SUSY threshold. The third and higher eigenfunctions display significant differences for both displayed η values. Remarkably, these differences diminish for higher eigenfunctions and for $n > 50$ the two eigenfunctions almost overlap in the displayed k_T region (relevant for a fit to HERA data). The reason for this can be seen from Fig. 8, which shows that for the relatively low transverse momenta the differences in the frequencies between the two models decrease with increasing eigenvalue number, so that if the infrared phases are equal, the functions will be almost identical in this region.

In summary we can state that the discrete BFKL pomeron shows a clear sensitivity to BSM physics effects and that these effects cannot be absorbed into its only free parameters, the infrared phase $\eta(\omega)$. This is clearly seen in the eigenvalue dependence on the SUSY thresholds, both in the LO analytical approach, Eqs. (2.28) and (2.43), and in the NLO numerical evaluation, Fig. 5. In addition, the asymptotic behaviour of the eigenvalues with increasing n (or decreasing ω) is very different for SM and SM+SUSY irrespective of the possible higher-order QCD corrections, Fig. 7. This means that we have here a very different situation from the scenario described by the decoupling theorem [7] where the large logarithmic corrections *can* be absorbed into unphysical renormalization constants leaving only higher dimension operators whose coefficients are suppressed by powers of the new-physics mass scale. In the case of the DP the effects of SUSY thresholds produce large changes of frequencies, Fig. 8, which modify the infrared perturbative phases η. These alter, in turn, the spectrum ω_n and hence the properties of the gluon density. Since the gluon density is a measurable quantity, the nonperturbative phases, η, can also be measured, although only indirectly.

3. COMPARISON WITH HERA DATA

3.1. General Considerations. One of the most important results of the HERA experiments is the measurement of the gluon density. This density encompasses the properties of the pomeron in the sense that the same gluon density determines the dynamics of the inclusive $\gamma^* p$ (or F_2) and diffractive processes, in particular the exclusive vector meson production. Several investigations performed in the context of the dipole models [18–25] have shown that the effective intercept of the gluon density measured by the rise of F_2 with diminishing x, called λ, is properly translated by the optical theorem, to the effective intercepts seen in the exclusive vector meson production.

The effective intercept λ measured at HERA varies from $\lambda \approx 0.2$ at $Q^2 = 10$ GeV^2 to about $\lambda = 0.35$ at $Q^2 = 100$ GeV^2, see Fig. 9 of [4]. The Q^2 dependence of λ in F_2 and in its diffractive counterparts can be well reproduced by the DGLAP evolution in which the values of λ are almost entirely of perturbative origin. In the well-known Donnachie–Landshoff (DL) [27] picture of the pomeron, the variation of λ with Q^2 is due to the existence of a hard ($\lambda = 0.4$) and a soft, nonperturbative, ($\lambda = 0.08$) pomeron whose admixtures vary with Q^2.

The properties of the gluon density corresponding to the DP are determined by the Green function constructed from the discrete eigenfunctions of the BFKL kernel (convoluted with the proton impact factor). In contrast to the DL pomeron, the DP is composed of many infinite eigenfunctions with eigenvalues varying like $\omega_n \approx 0.5/n$. The eigenvalues ω_n are almost entirely of perturbative origin because its only nonperturbative ingredients are the infrared phases η_n, which have a negligible importance for larger n, as was explained in the previous section.

The infrared phases have, however, a strong influence on the shape of the gluon density, since they determine how the contributing eigenfunctions add together. Let us recall that the unintegrated gluon density from the DP is of the form

$$\dot{g}(x,k^2)_{\rm DP} = \frac{1}{x}\,k^2 \sum_{n=1}^{n_{\max}} \left(\frac{k}{x}\right)^{\omega_n} A_n f_n(k,\eta_n), \tag{3.1}$$

where $\dot{g}$ means differentiation of the gluon density w.r.t. $\ln(k^2)$. Here, the eigenfunctions as a function of k (rather than t) are normalized w.r.t. k and are related to $f_n(t)$ by

$$f_n(k,\eta_n) = \frac{1}{k} f_n\left(\ln\left(\frac{k^2}{\Lambda^2_{\rm QCD}}\right)\right). \tag{3.2}$$

A_n is the overlap integral of these eigenfunctions with the proton impact factor, Eq. (3.3), with the eigenfunctions $f_n(k,\eta_n)$ computed with a specific $\eta - n$ relation, η_n (after accounting for the nonzero overlaps of the eigenfunctions of the non-Hermitian kernel, for detail, see [4]). The sum over eigenfunctions in Eq. (3.1) is limited for numerical reasons (see below) to $n_{\max} = O(100)^*$. The oscillation frequencies of the eigenfunctions, at transverse momenta relevant to HERA, vary very little from one eigenfunction to the next, so in order to obtain

*We have shown in [4] that an adequate description of HERA F_2 data requires $O(100)$ eigenfunctions. Nevertheless, the limit of $n_{\max} \sim 100$ represents a model assumption which is sufficient for HERA data but which could be too low for evaluation of LHC DY data. For LHC data it could also be necessary to include the contributions of negative ω's, Eq. (2.4).

a positive gluon density, which grows with k, it is necessary to generate a strong $\eta - n$ (or equivalently $\eta - \omega$) dependence; the eigenfunctions oscillate in $\ln k$, and the only way to cancel these oscillations is to introduce a shift of the phase between the different eigenfunctions.

The sum of Eq. (3.1) determines the evolution properties of the gluon density in agreement with the BFKL equation (1.1). The infrared phases are determined by the dynamics of nonperturbative QCD, and it should be possible, in principle, to estimate them using lattice calculations. It should also be possible to determine them directly from data at comparatively small Q^2. However, in order to be able to extract these phases accurately, the required data set should have a much larger x and Q^2 range than the presently available HERA measurements. In addition, the data set has to achieve the precision of the present HERA F_2 data.

Therefore, at present, to be able to confront the DP with data, we have no other choice but to construct a heuristic model for the infrared boundary condition based on the general understanding of the nonperturbative physics. We first postulate that the form of the infrared phase function, $\eta(\omega)$, dictated by the infrared behaviour of QCD, is *not* sensitive to BSM physics and is a smooth function of ω rather than an arbitrary number for each eigenfunction. We then choose to describe it in terms of a suitable parameterization, motivated by a similarity of the BFKL dynamics with the Schrödinger equation, described in detail below. In addition to the phases, we have also to specify the proton impact factor.

We consider this heuristic approach as a first step towards the determination of the infrared phases, which are important quantities of the nonperturbative QCD. The main purpose of the investigation reported in [4] was to check whether a physically plausible boundary condition provides a good description of data, i.e., whether the discrete BFKL pomeron can describe the dynamics of the measured gluon density. The main purpose of the present investigation is to find out whether the genuine sensitivity of the DP to the presence of BSM physics at high-energy can improve or worsen the quality of the fit to data, notwithstanding the uncertainties associated with the infrared phase conditions.

3.2. The Infrared Boundary. Our heuristic model of the infrared boundary consists of a set of physically well motivated assumptions about the proton impact factor and about the $\eta - n$ (or equivalently $\eta - \omega$) relation.

The proton impact factor has to be positive everywhere and concentrated at the values of $k < \mathcal{O}(1)$ GeV. We therefore choose a very simple possible form

$$\Phi_p(k) = Ak^2 \, \mathrm{e}^{-bk^2}, \tag{3.3}$$

as in [4]. We have also investigated other forms of the proton impact factor, e.g., with different powers of k^2 in the prefactor and/or the exponent but found that the fit to data has no sensitivity to such alternatives. This is due to the

fact that all eigenfunctions have a similar, oscillatory, shape near the infrared boundary and that the period of oscillations of the eigenfunctions is much larger than any physically possible support of the proton impact factor. Note that the form (3.3) vanishes as k^2 for small k, as required by colour transparency, and that the coefficient b has the interpretation of the average inverse square transverse momentum of partons inside the proton (the value of the parameter b was left though completely free in the fit).

Our choice of ansatz for the dependence of the infrared phases η_n on the eigenfunction number n is motivated from an examination of Eq. (2.28) for the eigenvalues at LO. We see that for large n we have $\omega_n \propto 1/n$ — the eigenvalues decrease and become closely packed as n increases. This is similar to the eigenvalues of a bound state in a Coulomb potential problem. The value of η_n has a restricted range (in order to avoid «cross-over» between adjacent eigenvalues), and its variation with n must be smaller than π. Since they are generated by the quasi-bound states of gluons inside the proton, they should be described by a simple parameterization. In [4], we found a simple, two-parameter, form

$$\eta_n = \eta_r \left(\frac{(n-1)}{(n_{\max}-1)} \right)^{\kappa}, \tag{3.4}$$

where $n_{\max}$ is the number of eigenfunctions we use for the fit and η_r represents the total range (in units of π). The parameter κ must be less than one. (Note that for $n_{\max} \to \infty$ and fixed n, the phase η_n formally tends to 0.)

Equation (3.4) is by no means unique, and we could have added terms which are analytic in ω_n of the form

$$b + c\omega_n + d\omega_n^2 + \ldots.$$

We have tested such more general parameterizations and found that, despite the introduction of extra parameters, there is no improvement in the quality of the fit obtained. We therefore use the simple ansatz (3.4), but we treat η_r as a free parameter (with the only restriction that it must not exceed one), in order to assure a bias-free evaluation in all of the fits that we perform.

In [4], we defined the infrared boundary as a phase condition at the lowest possible value of the transverse momentum, $k = k_0$, which can be safely reached by the perturbative calculation. To make this value as close as possible to $\Lambda_{\rm QCD}$, we considered only the one-loop running of the coupling. This gave a value of $k_0 = 0.3$ GeV, which corresponds to $\alpha_s \sim 0.7$. The reason for running the coupling at one loop only was that in principle this is the same order of perturbation theory as the NLO characteristic function χ_1 [9]. However, given that we modify the eigenvalue Eq. (2.52) by resumming all the large corrections in χ_1 using the technique of [10], it is more appropriate to take the β function to two-loop order which is what we use in this paper.

When we do this, we are faced with a problem — namely, that we cannot run the coupling below an «infrared» scale $k_0 = 0.6$ GeV, which corresponds to $\alpha_s \sim 0.7$ (at the two-loop level), without approaching the Landau pole too closely. On the other hand, the infrared boundary conditions are to be imposed at a transverse momentum of order $\Lambda_{\rm QCD}$. Moreover, we need to know the eigenfunctions below k_0 in order to perform a convolution with the proton impact factor, which has support mainly below k_0. Therefore, guided by the behaviour of the eigenfunctions in the perturbative region, we continue them down to a lower momentum $\tilde{k}_0$, which should be of order $\Lambda_{\rm QCD}$, using the extrapolation of the phase $\phi_n(k)$

$$\phi_n(\tilde{k}_0) = \phi_n(k_0) - 2\nu_n^0 \ln\left(\frac{k_0}{\tilde{k}_0}\right), \tag{3.5}$$

where for each eigenfunction, with index n, ν_n^0 is the frequency of the oscillations near $k = k_0$ [4]. We have assumed that this frequency is constant below k_0, an assumption which is correct for sufficiently small k_0, at least for the leading-order BFKL kernel (see [12]). Any deviation from constant frequency should have a negligible effect as we are only extrapolating over a small range in gluon transverse momentum. The numerical values of ν_n^0 are obtained by inverting the eigenvalue equation (2.52), modified according to [10].

The overlap integrals between the proton impact factor and the eigenfunctions must also start at $\tilde{k}_0$ (the support of these impact factors being significantly attenuated at k_0). We therefore use this momentum at which we impose the infrared phases of the eigenfunctions. The relation between the phases at k_0 and $\tilde{k}_0$ is given by Eq. (3.5). We leave the exact value of $\tilde{k}_0$ as a free parameter with the restriction that it must be $\mathcal{O}(\Lambda_{\rm QCD})$ and define it to be the scale at which the phase of the leading eigenfunction vanishes (as can be seen from Eq. (3.4)).

3.3. Results of the Fit. Before a comparison can be made with the measured structure function F_2, it is necessary to convolute the gluon density with the impact factor for the virtual photon (for details of the procedure, see Sec. 6 of [4]). The impact factor for the virtual photon is calculable in perturbative QCD and has support which is peaked at transverse momenta of the order of the photon virtuality, $\sqrt{Q^2}$.

The fits were performed using the HERA data [5] in the low-x region, $x < 0.01$. To avoid any saturation effects, we have limited the fit to the $Q^2 > 8$ GeV^2 region. We recall that the saturation scale at HERA was determined to be $Q_S^2 = 0.5$ GeV^2 at $x \approx 10^{-3}$ [23,24]; therefore, our choice of the Q^2 region is very conservative. This choice means that, in this paper, we concentrate on the one-pomeron exchange, without any multi-pomeron contributions, which could induce saturation effects. The saturation effects could also play a role without multi-pomeron effects through a modification of the boundary conditions, see [26], which in turn could modify our ansatz for the infrared boundary.

In any case, our choice of the Q^2 region for fits assures that saturation effects can be ignored in this first evaluation. In the future we plan to extend our analysis into the Q^2 regions which could be more sensitive to saturation.

In the region of $Q^2 > 8$ GeV^2, we have a total of 108 data points and a total of 5 parameters, so the number of degrees of freedom is $N_{\rm df} = 103$. We consider the $Q^2 > 8$ GeV^2 region as our main investigation region and use the $Q^2 > 4$ GeV^2 as a cross check.

As discussed in the previous paper [4], in order to obtain the most accurate estimate of the unintegrated gluon density, we should include in the fit as many of the higher n eigenfunctions as possible. Indeed, we observe that the fit quality improves with increasing number of included eigenfunctions and the series converges in χ^2. In principle, this convergence should improve as $n \to \infty$; however, in practice, the number of eigenfunctions used in a fit is limited by the numerical precision of our calculation. We have indications that, if we take significantly more than 100 eigenfunctions, our fit could be polluted by numerical instabilities arising from an accumulation of computational rounding errors. Moreover, we find no improvement in the quality of our fits, either in the case of the Standard Model or for MSSM SUSY at any of the thresholds investigated, when the maximum number of eigenfunctions $n_{\rm max}$ exceeds 100. We have therefore taken $n_{\rm max} = 100$ throughout.

Fits for $N = 1$ SUSY at different scales. The bottom row corresponds to the Standard Model. All fits are performed with $n_{\rm max} = 100$

SUSY scale, TeV	χ^2	κ	$\tilde{k}_0$, GeV	η_r	A	b, GeV^{-2}
3	125.7	0.555	0.288	–0.87	201.2	10.6
6	114.1	0.575	0.279	–0.880	464.8	15.0
10	109.9	0.565	0.275	–0.860	693.1	17.4
15	110.1	0.555	0.279	–0.860	882.2	18.6
30	117.8	0.582	0.278	–0.870	561.6	16.2
50	114.9	0.580	0.279	–0.870	627.4	16.8
90	114.8	0.580	0.279	–0.870	700.2	17.5
∞	122.5	0.600	0.294	–0.795	813.1	18.2

In the table we show our fits for various SUSY thresholds as well as the Standard Model. Let us first note that the $\tilde{k}_0$ values obtained in the unbiased fit, $\tilde{k}_0 \sim 275$ MeV, are close to $\Lambda_{\rm QCD}$. At the same time, the value of b implies that the proton impact factor peaks around $\Lambda_{\rm QCD}$, as expected for a self-consistent description. This, together with the relatively low χ^2's of all fits, confirms the success of our construction of the infrared boundary.

The quality of the fits shows a clear preference of the evaluation with SUSY effects; the fit for the Standard Model is worse than the fits with SUSY thresholds

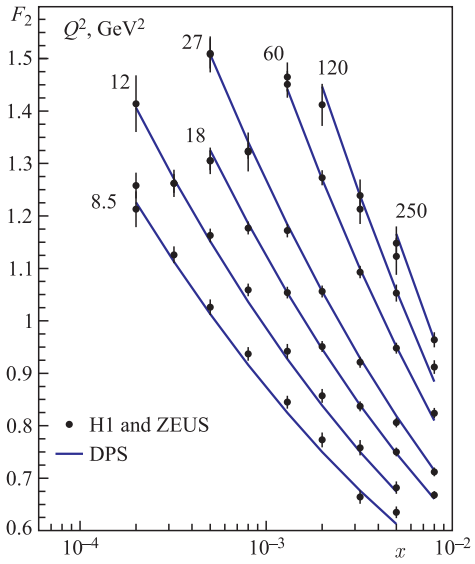

Fig. 11. Comparison of the DP fit with $M_{\mathrm{SUSY}} = 10$ TeV with HERA data

larger than 3 TeV. A SUSY threshold of 3 TeV, which is close to the reach of the LHC, also gives a worse fit. On the other hand, for a SUSY threshold in the region of 10–15 TeV, the quality of the fit is significantly improved, but that for significantly larger SUSY thresholds worsens again.

Let us note that the differences between the χ^2 fits shown in the table are very significant because the maximum-likelihood method, which assures that the minimum of χ^2 provides the best estimate of the parameter values, also states that 1σ error in determination of parameter values is given by $\Delta\chi^2 = 1$, irrespective of the number of degrees of freedom. Therefore, the differences between the fits of the table are a multi-σ effect, within our model of the infrared boundary.

The $\Delta\chi^2 = 1$ rule is valid as an estimate of the parameter error only for estimates within one theoretical framework, i.e., for one likelihood function. On the other hand, when χ^2 is used to quantify the agreement of different theories with data, it is expected that the observed χ^2 can deviate from the optimal value, because it fluctuates with the probability density function $f(\chi^2, N_{\mathrm{df}})$, which is approximately a Gaussian with the average value equal to N_{df} and the variance, $\sigma^2 = 2N_{\mathrm{df}}$. In the case of fits presented in the table, the expected χ^2 should be around 103 and $\sigma = 14$. Therefore, the χ^2 values obtained for best fits with the SUSY mass $\mathcal{O}(10)$ GeV lay well within one standard deviation. The DGLAP fits have a $\chi^2/N_{\mathrm{df}} \approx 0.95$. This would lead for our sample to $\chi^2 = 98$, which is also within one standard deviation of the optimal value, so that one cannot conclude

that either fit is better. The evaluation with the *goodness-of-fit* criterion called *p-value*, which is more appropriate for $N_{\rm df} \sim 100$, gives a *p-value* $\approx 30\%$ for SUSY masses of $\mathcal{O}(10)$ GeV, which is again an excellent result, see [16, 17].

As a check, we also performed the fits with a lower Q^2 cut, $Q^2 > 4$ GeV^2. We find that in this Q^2 region there is a significant increase of $\chi^2/N_{\rm df}$ presumably due to various higher order effects, such as the NLO contribution to the photon impact factor or valence quarks effects and possibly also the proximity of the saturation region. Although the overall quality of the fit for all data with $Q^2 > 4$ GeV^2 is significantly worse than with $Q^2 > 8$ GeV^2, the preference for $N = 1$ SUSY with the threshold region of 10–15 TeV is also clearly seen. In the $Q^2 > 4$ GeV^2 region there are 128 points and the χ^2's of the best fits are 184.3 (3 TeV), 164.5 (6 TeV), 155.6 (10 TeV), 152.6 (15 TeV), 169.7 (30 TeV), 164.7 (50 TeV), 164.3 (90 TeV). The best χ^2 for the Standard Model is 169.7. The values of the fit parameters are similar to the values shown in the table for the $Q^2 > 8$ GeV^2 region.

4. DISCUSSION

The main result of this paper, namely a possible sensitivity of HERA data to BSM effects, is especially astonishing as it was not seen in the usual solutions to the BFKL equation [1–3]. This sensitivity is due to the fact that we use the Green function method, in which the Green function is considered to be a universal property of the BFKL equation and that, apart from supplementing this equation with a given set of infrared boundary conditions for the eigenfunctions, no cuts on transverse momentum are applied, so that the conformal invariance is broken in a very smooth way, solely by the running of the coupling constant.

Had we imposed kinematic limits on the gluon virtuality for the individual eigenfunctions, then for those eigenfunctions with $\omega \lessapprox 0.1$, they would never reach the region in which they decay as required for compatibility with a DGLAP analysis in the DLL limit. Alternatively, one might attempt to fit HERA data only with the first eigenfuction, which does indeed start to decay within the HERA region, making the assumption that the higher eigenfunctions (with lower ω) only couple weakly to the proton. However, the properties of this first eigenfunction are in clear contradiction with data; for example, the rate of raise of F_2 with diminishing x would be independent of Q^2 with a value of $\lambda \approx 0.25$, whereas the λ value in data varies between 0.15 and 0.35 in the observed Q^2 region. The results of [11] indicate that one needs at least four eigenfunctions to describe HERA data (making an artificial assumption that the overlap constants A_n of Eq. (3.1) are totally unconstrained), which extends the virtuality region to $k_c^{(4)} \sim 1000$ TeV.

In the solution which we have adopted, the momentum conservation is incorporated by convoluting the Green function with the proton form factor as defined by the solution of the BFKL Eq. (1.1)

$$\mathcal{WP}(y,k^2) = \int d\omega \int \frac{dk'^2}{k'^2}\, \mathrm{e}^{\omega y}\, \hat{\mathcal{G}}_\omega(k,k')\, \Phi_p(k'), \tag{4.1}$$

where in analogy to Eq. (3.1) the Green function $\hat{\mathcal{G}}_\omega(k,k')$ is written in terms of the eigenfunctions $f_n(k,\eta_n)$ and $f_n(k',\eta_n)$. This expression describes the evolution of a wave packet, $\mathcal{WP}$, from the rapidity $y=0$ to the larger rapidity y values*. The (approximate) momentum conservation emerges here because the quasi-local nature of the kernel $\mathcal{K}(t,t')$ ensures that there is no evolution into the very large transverse momenta, apart from the usual BFKL diffusion, $\ln k_T \sim \sqrt{\alpha \ln s}$. Figure 12 shows the wave packet as it evolves from the smallest to the largest rapidity values of the HERA region, $y = \ln(1/x)$, and for the SM and SM+SUSY cases.

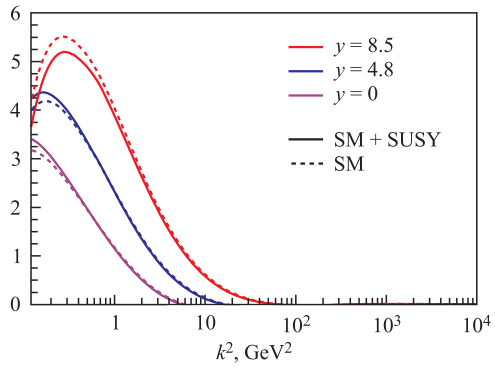

Fig. 12. Evolution of the initial wave packet in the DP solution of the BFKL equation as determined from the fit to HERA F_2 data

The initial wave packet, the curve $\mathcal{WP}(y=0,k^2)$ shown in Fig. 12, is not quite the same as the function $\Phi_p(k)$ defined in Eq. (3.3) (divided by k^2), but rather it is related to it by Eq. (4.1); i.e., it is built only out of the eigenfunctions which obey the imposed boundary conditions on the Green function. For large y, it is sufficient to consider only the discrete eigenvalue part of the Green function in Eq. (4.1), and so we are actually using that part of the proton impact factor which is orthogonal to the (continuum) negative ω eigenfunctions. The

*Note that the analogy to the QM wave packet is not complete because in the BFKL equation rapidity is analogous to imaginary time.

initial wave packet is somewhat broader than the distribution of Eq. (3.3), but it has the required features that it is localized to the transverse momenta of ~ 1 GeV. With increasing rapidity it broadens due to the BFKL diffusion, but this broadening remains moderate, of a size of just few GeV, as in the usual solutions of the BFKL equation. Although our kernel is constructed from the oscillating eigenfunctions with properties determined by the BFKL dynamics at very high transverse momenta, the oscillations cancel away due to the choice of the phases η_n in the fit procedure, and what remains is only a slight broadening of the gluon diffusion spectrum with increasing y.

In the application to DIS it is more customary to consider the evolution of the unintegrated gluon density given by

$$x\dot{g}(x,k^2) = k^2 \int d\omega \int \frac{dk'^2}{k'^2} \left(\frac{kx}{k'}\right)^{-\omega} \hat{\mathcal{G}}_\omega(k,k')\,\Phi_p(k'), \tag{4.2}$$

which differs from the evolution of the wave packet, Eq. (4.1), by the kinematical factor k^2 and the factor $(k/k')^{-\omega}$. The latter factor encodes the difference beween Bjorken-x and rapidity, y. It is close to one and of minor importance. On the other hand, the factor of k^2 is important as it amplifies the high virtuality contributions to the structure function (note that F_2 is obtained from a convolution of the unintegrated gluon density with the photon impact factor which selects k^2 values close to the Q^2 of the experiment).

In Fig. 13 we show the unintegrated gluon density at two values of x — one in the middle of HERA region, $x = 10^{-3}$, and the other just above HERA low-x region, $x = 10^{-4}$. The figure shows again that the contribution of BSM physics changes the shape of the gluon density but does not lead to an increase of the large transverse momentum tail (in fact, this tail turns out to be smaller for SM + SUSY) contrary to the naive expectation that BSM effects should show

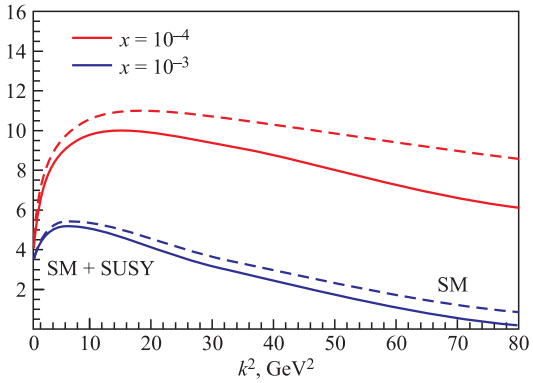

Fig. 13. The unintegrated gluon density using the DP solution of the BFKL equation, as determined from the fit to HERA F_2 data

up as an increased parton activity at large virtualities. The figure also shows that the discrepancy between the unintegrated gluon density for the SM alone and for SM + SUSY increases substantially with diminishing x at larger k^2, which suggests that Drell–Yan measurements at the LHC, in the region of $x \sim 10^{-4}$ and $k^2 \sim 50$ GeV^2, could have high sensitivity to BSM physics.

In contrast to the diffusion effect, the important point that we are stressing is that it is the spectrum of allowed eigenvalues (and also the shape of the eigenfunctions) that enters into the construction of the Green function which is sensitive to physics at high scales. This sensitivity emerges from the interplay of two main features of the DP solution: the identity of the boundary condition in respect to addition of $n\pi$ to the phase and the running of the coupling constant. For $n \geqslant 3$ this interplay is affected by SUSY effects, whereas for $n \leqslant 2$ the eigenvalues are unaffected since the critical transverse momentum t_c is below the SUSY threshold. For $n \geqslant 3$, the change of the eigenvalues is substantial. As n increases, the ratio of eigenvalues with and without SUSY rapidly reaches its asymptotic value of 7/3. In Fig. 14 we compare the summed contribution of the eigenfunctions which are sensitive to BSM effects ($n = 3, \ldots, 100$) with the sum of contributions of the first two eigenfunctions which are not sensitive to SUSY. The contributions of the $n = 3, \ldots, 100$ eigenfunctions change both in size and in shape when evaluated with and without SUSY, whereas the contribution of the first two eigenfunctions remains unaltered.

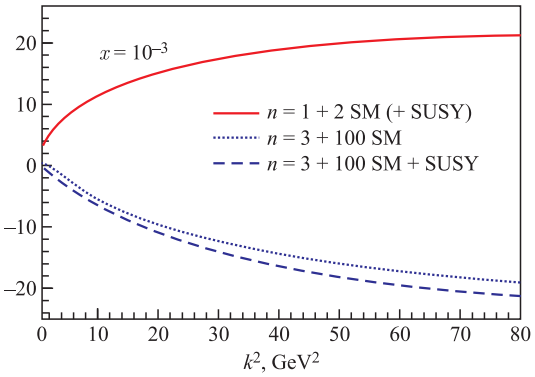

Fig. 14. Comparison of contributions to the unintegrated gluon density from the eigenfunctions which are not sensitive ($n = 1, 2$) and which are sensitive to BSM effects ($n = 3, \ldots, 100$) to the curve at $x = 2 \cdot 10^{-3}$ of Fig. 11

Figure 15 shows the η variation as a function of the eigenvalue ω for the fit with the SUSY threshold of 10 TeV and for the SM fit only. Both relations show a substantial variation of the phase η with decreasing ω. The substantial difference between the two relations reflects a large difference between the eigenvalues and eigenfunctions in both cases.

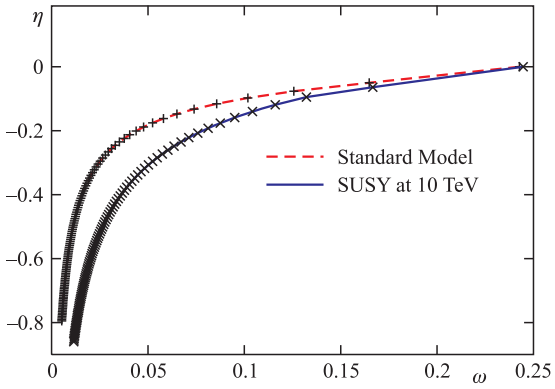

Fig. 15. The eigenvalues and infrared phases for the Standard Model and $N = 1$ SUSY at 10 TeV, as determined at $k = \tilde{k}_0$

The changes due to BSM effects lead to a substantial increase of χ^2 when the corresponding gluon densities are confronted with data, because the changes are of the order of 10%, whereas the data precision is around 1–2%. Indeed, the evolution of the unintegrated gluon density performed with the SM alone, using the same parameter values for η boundary as in the SUSY case (dotted line in Fig. 14, dashed lines in Fig. 13), would give an increase of χ^2 by $\Delta\chi^2 \sim 160$ when compared to data. On the other hand, had we used the η boundary parameters as determined with the SM alone and performed the evolution with the SM + SUSY eigenvalues and eigenfunction, the increase of χ^2 would be even larger, $\Delta\chi^2 \sim 300$. The differences between the χ^2's of the SM and SM + SUSY fits shown in the table are substantially smaller, $\Delta\chi^2 \sim 12$, because the parameters of the η boundary conditions and the proton form factors were fitted to data, which diminishes substantially the sensitivity to BSM effects.

It is quite clear that the DP could provide an exciting framework to study BSM effects if more can be learned about its infrared boundary. One way to improve our knowledge of this boundary is to apply our analysis to another, independent set of data, such as the Drell–Yan processes at the LHC*. The LHC Drell–Yan data extend in the low-x region to much larger Q^2 scales than HERA data. This will allow the study of the evolution in $\ln k^2$ which is dominated in the DP scheme by the low-ω region. This region and the region of very low x are very sensitive to SUSY effects and at the same time are much less sensitive to NLO effects which are difficult to compute.

*Natural candidates would also be the diffractive HERA processes. Unfortunately, they are not measured with sufficient accuracy because the HERA detectors were not designed to measure diffractive processes.

Future HEP experiments, which are now under discussion, can also substantially improve the knowledge of the infrared boundary and of the properties of the DP. The LHeC project [28] could provide important information about the region of very low x and not so high scales. This could lead to a better understanding of the properties of the large ω contributions. In addition, it will also be possible to measure precisely the exclusive diffractive processes. This will provide an independent evaluation of the infrared boundary since in the exclusive processes (e.g., in the exclusive J/ψ or Υ production) the gluon density contributes almost in square [21, 23].

The properties of the DP can also be studied very well in the $\gamma^*\gamma^*$ process in a future linear e^+e^- collider [29]. The $\gamma^*\gamma^*$ process is very interesting because it would permit the direct test of the universality of the BFKL pomeron and its boundary condition. Of particular interest could also be the newly proposed electron wake field accelerator [30], which could accelerate electrons into the several-TeV energy region. This would allow the measurement of the $\gamma^*\gamma^*$ structure function at very low x and high Q^2's, which could further increase the sensitivity to BSM effects.

5. SUMMARY

In this paper we have analyzed the properties of the Discrete BFKL Pomeron (DP), using analytical and numerical methods. We show, using as example $N = 1$ SUSY, that BSM physics substantially alters its eigenvalue spectrum and the shape of its eigenfunctions. This is a genuine sensitivity insofar as it cannot be entirely absorbed into any free parameters of the discrete pomeron solution of the BFKL equation.

The physical origin of this sensitivity can be traced back to the fact that in the low Bjorken-x regime the behaviour of the structure functions is directly related to the positions of the Regge poles (pomerons). In the BFKL approach, due to the approximate conformal invariance, the corresponding eigenfunctions and eigenvalues of the BFKL kernel are determined from exponentially large transverse momenta, where contributions from particles of any BSM physics play an essential role. On the other hand, the locality property of the BFKL equation assures that, in any physical process performed at energy scales which are much lower than the BSM ones, the BSM quanta cannot be produced and the transverse momenta of the virtual particles are very limited. The effects of large transverse momenta appear, however, through the substantial alteration of the eigenstate spectrum of the BFKL Hamiltonian, which is important in the low-x region. In our view, this provides a new mechanism for the detection of BSM effects, which has not previously been considered.

The eigenvalue spectrum of the DP cannot be directly measured because it determines the gluon density through a complicated superposition of pomeron

states. The result of their interference can be compared with data only after the free parameters of the BFKL solution, determining the infrared boundary, are specified. Although the infrared boundary is a physical quantity of nonperturbative QCD origin, we could only determine it in this and the previous paper within a heuristic approach. Our description of this boundary provides a very good fit to the data and shows that the BSM effects are sensed by the HERA F_2 data, notwithstanding the large freedom of the parameter choice.

The analysis of HERA data indicates an improved quality of fit for the case of $N = 1$ SUSY, with the SUSY scale as being around 10 TeV. Needless to say that this determination is only possible within our heuristic model approach. Our limited knowledge of the infrared boundary diminishes substantially (but not completely) the sensitivity of the fit to BSM effects.

This sensitivity can be substantially improved by a better determination of the universal boundary condition. We can gain a better understanding of the infrared boundary from the analysis of additional data sets, especially of the LHC Drell–Yan data. The data from the future experimental facilities like LHeC, the e^+e^- linear collider or even higher energy plasma wake field accelerators could also become crucial. The $\gamma^*\gamma^*$ process which can be very well measured at the linear colliders is of particular interest, since in this reaction the properties of the discrete pomeron solution are simplified owing to the absence of the proton.

The method described in this paper opens a new possibility of using high-precision experiments to search for new physics at energy scales considerably larger than the scales at which the experiments are performed. We consider the approach formulated here, which involves a heuristic model for the parameterization of the infrared phases of the BFKL eigenfunctions, as a first step which should be substantially improved by involving more data and more theoretical analysis.

Acknowledgements. The authors are grateful to the Marie Curie Foundation for an IRSES grant, LOWXGLUE Project 22498, which has facilitated this collaboration. We wish to thank the St. Petersburg Nuclear Physics Institute and Southampton University for their hospitality while this work was carried out.

We are grateful to J. Bartels for illuminating and useful discussions about the physical interpretation of the discrete BFKL pomeron. We would like to thank A. Mueller for a careful reading of the manuscript and encouragement. We are also grateful to A. Caldwell, A. Geiser, E. Lohrmann and R Mankel for useful discussions about the meaning of χ^2 tests. We also thank J. Ellis and A. Weiler for lively discussions.

REFERENCES

1. *Askew A. J. et al.* // Phys. Rev. D. 1994. V. 49. P. 4402.
2. *Kwiecinski J., Martin A. D., Stasto A. M.* // Phys. Rev. D. 1997. V. 56. P. 3991.
3. *Ciafaloni M. et al.* // Phys. Rev. D. 2003. V. 68. P. 114003.

4. *Kowalski H. et al.* // Eur. Phys. J. C. 2010. V. 70. P. 983; Nucl. Phys. A. 2011. V. 854. P. 45.
5. *Aaron F. D. et al. (H1 and ZEUS Collab.).* Combined Measurement and QCD Analysis of the Inclusive ep Scattering Cross Sections at HERA // JHEP. 2010. V. 1001. P. 109.
6. *Balitsky I. I., Lipatov L. N.* The Pomeranchuk Singularity in Quantum Chromodynamics // Sov. J. Nucl. Phys. 1978. V. 28. P. 822;
Kuraev E. A., Lipatov L. N., Fadin V. S. Multi-Reggeon Processes in the Yang–Mills Theory // Sov. Phys. JETP. 1976. V. 44. P. 443;
Fadin V. S., Kuraev E. A., Lipatov L. N. // Phys. Lett. B. 1975. V. 60. P. 50.
7. *Appelquist T., Carrazonne J.* // Phys. Rev. D. 1975. V. 11. P. 2856.
8. *Grzadkowski B., Krawczyk P., Pokorski S.* // Phys. Rev. D. 1984. V. 29. P. 1476.
9. *Fadin V. S., Lipatov L. N.* BFKL Pomeron in the Next-to-Leading Approximation // Phys. Lett. B. 1998. V. 429. P. 127;
Ciafaloni M., Camici G. Energy Scale(s) and Next-to-Leading BFKL Equation // Phys. Lett. B. 1998. V. 430. P. 349.
10. *Salam G. P.* A Resummation of Large Sub-leading Corrections at Small x // JHEP. 1998. V. 9807. P. 019.
11. *Ellis J., Kowalski H., Ross D. A.* Evidence for the Discrete Asymptotically Free BFKL Pomeron from HERA Data // Phys. Lett. B. 2008. V. 668. P. 51.
12. *Lipatov L. N.* The Bare Pomeron in Quantum Chromodynamics // Sov. Phys. JETP. 1986. V. 63. P. 904.
13. *Adloff C. et al. (H1 Collab.).* Deep-Inelastic Inclusive ep Scattering at Low x and a Determination of Alpha(s) // Eur. Phys. J. C. 2001. V. 21. P. 33;
Chekanov S. et al. (ZEUS Collab.). Measurement of the Neutral Current Cross Section and F_2 Structure Function for Deep Inelastic e^+p Scattering at HERA // Ibid. P. 443.
14. *Kotikov A. V., Lipatov L. N.* NLO Corrections to the BFKL Equation in QCD and in Supersymmetric Gauge Theories // Nucl. Phys. B. 2000. V. 582. P. 19; DGLAP and BFKL Evolution Equations in the $N = 4$ Supersymmetric Gauge Theory // Nucl. Phys. B. 2003. V. 661. P. 19.
15. *Martin A. D. et al.* Parton Distributions for the LHC // Eur. Phys. J. C. 2009. V. 63. P. 189.
16. *Beaujean F. et al.* // Phys. Rev. D. 2011. V. 83. P. 012004.
17. *Blobel V., Lohrmann E.* Statistische und numerische Methoden der Datenanalyse von Volker Blobel und Erich Lohrmann. Teubner Studienbuecher, 1998.
18. *Golec-Biernat K., Wuesthoff M.* // Phys. Rev. D. 1999. V. 59. P. 014017; V. 60. P. 114023.
19. *Munier S., Staśto A. M., Mueller A. H.* Impact Parameter Dependent S-matrix for Dipole Proton Scattering from Diffractive Meson Electroproduction // Nucl. Phys. B. 2001. V. 603. P. 427.
20. *Bartels J., Golec-Biernat K., Kowalski H.* A Modification of the Saturation Model: DGLAP Evolution // Phys. Rev. D. 2002. V. 66. P. 014001.

21. *Kowalski H., Teaney D.* // Phys. Rev. D. 2003. V. 68. P. 114005.

22. *Forshaw J. R., Sandapen R., Shaw G.* Colour Dipoles and Rho, Phi Electroproduction // Phys. Rev. D. 2004. V. 69. P. 094013.

23. *Kowalski H., Motyka L., Watt G.* // Phys. Rev. D. 2006. V. 74. P. 074016.

24. *Watt G., Kowalski H.* // Phys. Rev. D. 2008. V. 78. P. 014016.

25. *Kowalski H. et al.* // Phys. Rev. C. 2008. V. 78. P. 045201.

26. *Mueller A. H., Triantafyllopoulos D. N.* // Nucl. Phys. B. 2002. V. 640. P. 331.

27. *Donnachie A., Landshoff P. V.* // Phys. Lett. B. 1998. V. 437. P. 408 (and references therein).

28. LHeC Conceptual Design Report. 2012.

29. The International Linear Collider Physics and Detector: 2011 Status Report.

30. *Caldwell A., Lotov K.* // Phys. Plasmas. 2011. V. 18. P. 103101.